Inorganics **2015**, *3*, 160-177; doi:10.3390/inorganics3020160

OPEN ACCESS

inorganics

ISSN 2304-6740

www.mdpi.com/journal/inorganics

Review

Polyoxoniobates and Polyoxotantalates as Ligands—Revisited

Pavel A. Abramov [1,2,*], Maxim N. Sokolov [1,2] and Cristian Vicent [3]

[1] Nikolaev Institute of Inorganic Chemistry SB RAS, Novosibirsk 630090, Russia; E-Mails: abramov@niic.nsc.ru (P.A.); caesar@niic.nsc.ru (M.N.)

[2] Novosibirsk State University, Novosibirsk 630090, Russia

[3] Serveis Centrals d'Instrumentació Científica, Universitat Jaume I, Av. Sos Baynat s/n, 12071 Castelló, Spain; E-Mail: barrera@sg.uji.es

* Author to whom correspondence should be addressed; E-Mail: abramov@niic.nsc.ru; Tel.: +7-383-316-58-45; Fax: +7-383-330-94-89.

Academic Editors: Greta Ricarda Patzke and Pierre-Emmanuel Car

Received: 8 April 2015 / Accepted: 8 May 2015 / Published: 20 May 2015

Abstract: This short review summarizes our contribution to the coordination chemistry of noble metals (organometallic fragments of Rh, Ir, Ru and hydroxo Pt(IV)) and polyoxocomplexes of niobium and tantalum.

Keywords: polyoxoniobates; tantalates; noble metals; 1H DOSY NMR; capillary electrophoresis

---

1. Introduction

The group 5 (V, Nb, Ta) polyoxometalates (commonly defined as anionic polynuclear oxocomplexes) form two large but apparently distinct families, which, despite certain resemblance, show almost no overlap [1–9]. Vanadium(V) prefers aggregation into decaniobate $[V_{10}O_{28}]^{6-}$ and rearrangement of this very stable structure (search in CBSD yields about 150 structurally characterized salts of this anion with various organic cations) can be realized only in the presence of PO_4^{3-} as template at low pH, producing a "bicapped" Keggin-type $[PV_{14}O_{42}]^{9-}$ anion [10–15]. Vanadium (IV) (but not Nb(IV) or Ta(IV)) can aggregate around differently-shaped anionic templates (like Cl^-, NCS^- *etc.*) producing a family of reduced polyoxovanadates built from tetragonal pyramids, with fascinating magnetic properties [16,17]. The chemistry of polyoxoniobates (PONb) and tantalates is much less

studied and for a long time it was confined to preparations of alkali metal salts of hexaniobate and hexatantalate, $[Nb_6O_{19}]^{8-}$ and $[Ta_6O_{19}]^{8-}$. The beginning of the modern era in this chemistry can be dated back to the works of Spinner, Pope and Stucky in the late 1960s–1980s [18–24], who obtained evidence for condensation of $[Nb_6O_{19}]^{8-}$ into larger entities, and discovered its ability to coordinate certain transition metals. This chemistry is quite different from polyvanadates and is dominated by Lindqvist hexametalates $[M_6O_{19}]^{8-}$, in spite of the existence of the decaniobate, $[Nb_{10}O_{28}]^{6-}$ [25,26] and recently reported decatantalate $[Ta_{10}O_{28}]^{6-}$ [27]. By contrary, free $[V_6O_{19}]^{8-}$ is unknown, and the reason for this is perhaps that, if existed, it would have an extraordinarily high charge density (defined as the anionic charge of the POM divided by the number of non-hydrogen atoms of the POM). Among the known POM, the highest charge density (0.32) is achieved precisely for $[M_6O_{19}]^{8-}$ [9]. As V is smaller than Nb, $[V_6O_{19}]^{8-}$ would have the highest charge density per volume ratio. It can be stabilized only by coordination of four positively charged $\{Cp^*Rh\}^{2+}$ units [28,29].

The high charge density means that $[M_6O_{19}]^{8-}$ anions are expected to act as efficient ligands towards various metals. This is indeed so, and a few examples of coordination of $[Nb_6O_{19}]^{8-}$ to Mn(IV) and Ni(IV) were reported, as early as in 1967–1969 [18–24], and Co(III), reported only in 2011 [30], giving complexes of the type $[M(Nb_6O_{19})_2]^{n-}$, where two hexaniobate units (each acting as tridentate ligand) sandwich an octahedrally coordinated central metal ion. There is also a strong association of hexaniobate with alkali metal cations, even in water, where the existence of neutral $[A_8Nb_6O_{19}]$ (A = Rb, Cs) species was established by Small Angle X-ray Scattering (SAXS) [31]. Curiously enough, no tantalate analogues of $[M(Nb_6O_{19})_2]^{n-}$ could be obtained [32]. It is doubtless highly desirable to expand this still rather modest list of existing complexes. However, strongly basic conditions, necessary to prevent hydrolysis of hexaniobate (and precipitation of niobium oxide), severely limit the choice of suitable metal precursors (they would simply give insoluble hydroxides). This drawback can be obviated in two different ways. First, in order to limit the hydrolysis and ensuing condensation, a part of the coordinating positions of a transition metal can be occupied by a polydentate (or polyhaptic) ligand (or simply by a strongly coordinated unidentate ligand, such as CO). This can be achieved for Co(III), Cr(III), Cu(II) and Ni(II) in the presence of polyamines [33–37]. Particularly attractive for this purpose are the isolobal fragments d^6-*fac*-$\{ML_3\}$, where ML_3 stands for $\{M(CO)_3\}^+$ (M = Mn, Re), $\{(arene)Ru\}^{2+}$, $\{Cp^*Rh\}^{2+}$, $\{Cp^*Ir\}^{2+}$. In fact, a decade ago Pope *et al.* used $[M_6O_{19}]^{8-}$ (M = Nb, Ta) as robust inorganic tridentate ligands in reactions with $[Mn(CO)_3(CH_3CN)_3]ClO_4$ or $[Re(CO)_5Br]$, which gave rise to *trans*-$[(M'(CO)_3)_2M_6O_{19}]^{6-}$ (M' = Mn, Re; M = Nb, Ta) [38]. Proust *et al.* reported the syntheses of a series of complexes combining $\{(arene)Ru\}^{2+}$ and $[Nb_6O_{19}]^{8-}$ with Ru/POM stoichiometries ranging from 1:1–4:1 [39]. Coordination of organometallic fragments, such as $\{(p\text{-cymene})Ru\}^{2+}$ or $\{Cp^*Rh\}^{2+}$, to POM adds extra possibilities for the synthesis of hybrid (*i.e.*, combining chemically very different moieties within the same structure) complexes. This development reflects not only academic interest in such compounds, being a logical development of POM chemistry in general, but also is driven by the well-known catalytic properties of many POM complexes of transition metals, in particular, with noble metals [40].

The second way is to use a metal which forms stable well-defined and water soluble hydroxocomplexes, such as Pt(IV), for which both $[Pt(OH)_4(H_2O)_2]$ and $[Pt(OH)_6]^{2-}$ exist as individual species [41]. In this case, a particular attraction for coordinating Pt(IV) to $[Nb_6O_{19}]^{8-}$ comes from the reports about use of PONb in photocatalysis. In this case, a photoactivator is necessary, which role is

typically fulfilled by $[PtCl_6]^{2-}$ [42]. From this point of view, direct coordination of Pt(IV) to PONb is very desirable. Pt(IV), being octahedral and sufficiently oxophilic, could either substitute a Nb atom in the hexaniobate structure, similar to $[H_2Pt^{IV}V_9O_{28}]^{5-}$ which is simply a Pt(IV)-monosubstituted classical decavanadate [43,44], or be "grafted" as a capping atom. As we will see, the latter is the case.

In this short review, we focus on the recent advances in the field of group V (in particular, Nb and Ta) POM complexes, concentrating on the synthesis of Lindqvist-based POM with incorporated noble metal centers and their potential applications as electrocatalysts for water oxidation. The second part addresses related studies with heteropolyniobiate homologues coordinating noble metal fragments. The third part deals with the current use of analytical tools to unravel the integrity and reaction dynamics in the solution and selected examples are discussed.

2. Reactivity of $[M_6O_{19}]^{8-}$ towards Noble Metal Complexes

In this section, studies of reactivity of the Lindqvist $[M_6O_{19}]^{8-}$ (M = Ta and Nb) POM towards a noble metal complex are discussed, with an emphasis on finding suitable experimental conditions for noble metal grafting, the main structural features of the resulting solids, as well as their behavior in aqueous solution.

2.1. Reaction $[M_6O_{19}]^{8-}$ with $\{Cp^*Rh\}^{2+}$ and $\{Cp^*Ir\}^{2+}$

Heating of $[Cp^*RhCl_2]_2$ with $K_7H[Nb_6O_{19}]\cdot 13H_2O$ or $Cs_8[Ta_6O_{19}]\cdot 14H_2O$ in water at 80–90 °C in 2:1 molar ratio yields yellow-orange solutions, from which $K_4[\{Cp^*Rh\}_2Nb_6O_{19}]\cdot 20H_2O$ (**1**) and $Cs_4[\{Cp^*Rh\}_2Ta_6O_{19}]\cdot 18H_2O$ (**2**) can be readily isolated in high yields (80% for Nb and 70% for Ta) [45]. Crystal structures of both complexes contain hybrid bi-capped organometallic-POM anions *trans*-$[\{Cp^*Rh\}_2M_6O_{19}]^{4-}$ (Figure 1) with the typical Lindqvist-type oxide metal core (metal octahedron with one μ_6-, twelve μ_2- and six terminal oxygen ligands) decorated at an opposite pair of the triangular $\{M_3O_3\}$ faces with two capping organometallic fragments $\{Cp^*Rh\}^{2+}$. In both cases, exclusively *trans*-isomers crystallize. No *cis*-isomers were observed in solution or in solid. Both **1** and **2** produce basic solutions in water; 3 mM solutions have the pH value of 8.8, which is much lower in comparison to that produced by alkali metal salts of parent $[M_6O_{19}]^{8-}$ of comparable concentration (10.5–11.0). The ESI(-) mass spectra of aqueous solutions of **1** and **2** display prominent peaks assigned to the $[\{Cp^*Rh\}_2M_6O_{19} + 2H]^{2-}$ dianions, accompanied by minor signals from the singly-charged $[\{Cp^*Rh\}_2M_6O_{19} + 3H]^{-}$ anions. However, the protonation degree observed by ESI-MS does not necessarily mirrors that in the solution because of the influence of the ESI process itself on the protonation [46]. For example, the most efficient ionization mechanism observed by ESI-MS for the decaniobate $[Nb_{10}O_{28}]^{6-}$ ion was the uptake of up to three protons, whereas solution studies indicated no protonation [26,47].

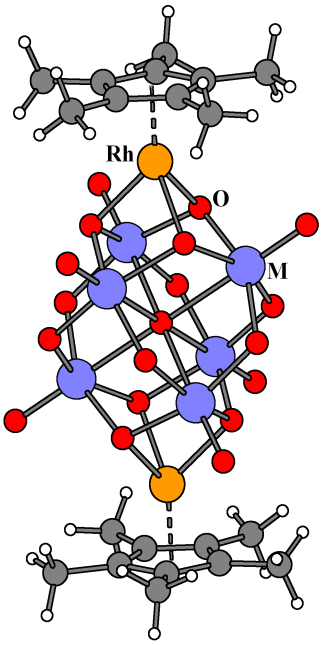

Figure 1. View of *trans*-$[\{Cp^*Rh\}_2M_6O_{19}]^{4-}$ in the crystal structure of $K_4[(Cp^*Rh)_2Nb_6O_{19}]\cdot 20H_2O$ (**1**) and $Cs_4[(Cp^*Rh)_2Ta_6O_{19}]\cdot 18H_2O$ (**2**) (ball and stick model).

The reactions of $[M_6O_{19}]^{8-}$ with $[Cp^*RhCl_2]_2$ in 1:1 molar ratio under the same conditions gave solutions, from which only poorly diffracting yellow solids could be isolated. These solids can be extracted with methanol yielding yellow solutions. The ESI mass spectra of the methanolic extracts were consistent with the presence of POM/Rh complexes featuring 1:1 stoichiometry of general formula ($[\{Cp^*Rh\}M_6O_{19}]^{6-}$ (**3**, M = Nb; **4**, M = Ta).

Grafting of $\{Cp^*Ir\}^{2+}$ fragments onto the $[M_6O_{19}]^{8-}$ (M = Nb, Ta) proceeds essentially in the same manner with $[Cp^*IrCl_2]_2$ as the source of the $\{Cp^*Ir\}^{2+}$ fragment. Both 2:1 $[\{Cp^*Ir\}_2Nb_6O_{19}]^{4-}$ (**5**, M = Nb; **6**, M = Ta) and 1:1 $[\{Cp^*Ir\}Nb_6O_{19}]^{6-}$ (**7**, M = Nb; **8**, M = Ta) complexes can be produced in high yields by varying the reagent ratio. In this case, we succeeded in isolation and X-ray characterization of potassium (M = Nb) and sodium (M = Nb, Ta) salts of 2:1 *trans*-$[\{Cp^*Ir\}_2M_6O_{19}]^{4-}$, and sodium salts of the single-capped $[\{Cp^*Ir\}M_6O_{19}]^{6-}$ complexes (both for Nb and Ta) (Figure 2).

Compound $\mathbf{5}^{4-}$ was tested as electrocatalyst for water oxidation. The cyclic voltammogram of the *trans*-$[\{Cp^*Ir\}_2Nb_6O_{19}]^{4-}$ ($\mathbf{5}^{4-}$) in 1 M Na_2SO_4 exhibited a strong anodic current due to water oxidation already at 0.8 V *versus* Ag/AgCl. The current (296 μA) at 1.6 V in the presence of the complex was 5.1 times higher than that (57.7 μA) for the blank solution.

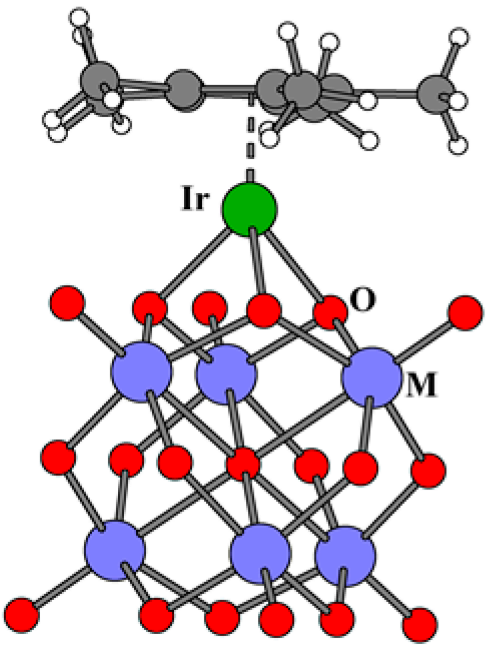

Figure 2. Ball and stick model of single-capped $[\{Cp^*Ir\}M_6O_{19}]^{6-}$ hybrid anions (M = Nb, Ta).

2.2. Complexation of $[Ta_6O_{19}]^{8-}$ with $\{(C_6H_6)Ru\}^{2+}$

$Na_8[Ta_6O_{19}]\cdot 24.5H_2O$ reacts with $[(C_6H_6)RuCl_2]_2$ (POM/Ru ratio 1:1) in water, yielding a yellow solution which contains single-capped $[(C_6H_6)RuTa_6O_{19}]^{6-}$ (**9**$^{6-}$) complex as the main product [48]. The progress of the reaction was monitored by ESI-MS as shown in Figure 3.

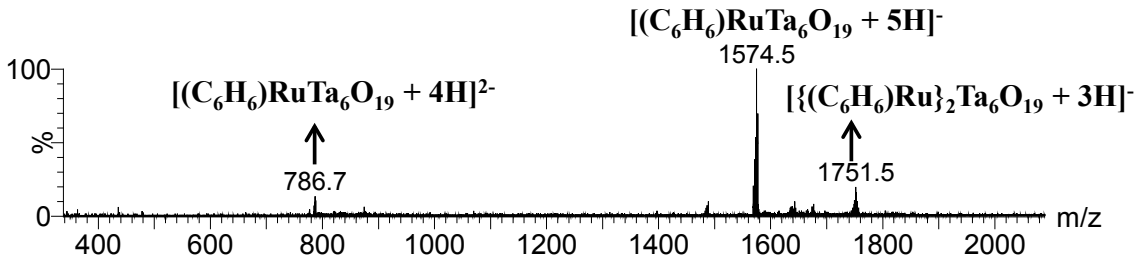

Figure 3. ESI(−) mass spectrum of aqueous solutions recorded at Uc = 10 V of the products of reaction between $Na_8[Ta_6O_{19}]\cdot 24.5H_2O$ and $[(C_6H_6)RuCl_2]_2$ with POM / Ru ratio 1:1.

The ESI(−) mass spectrum of this reaction features the $[(C_6H_6)RuTa_6O_{19} + 5H]^-$ anion (*m/z* 1574.5) as the base peak, accompanied by a minor signal due to the doubly charged $[(C_6H_6)RuTa_6O_{19} + 4H]^{2-}$ species (*m/z* 786.7). A minor peak at *m/z* 1751.5 was attributed to the double-capped $[\{(C_6H_6)Ru\}_2Ta_6O_{19} + 3H]^-$ anion with two coordinated $\{(C_6H_6)Ru\}^{2+}$ units. Evaporation of the reaction solution gave yellow plates of $Na_{10}[\{(C_6H_6)RuTa_6O_{18}\}_2(\mu\text{-}O)]\cdot 39.4H_2O$ (**10**) in 80% yield, with unexpected $[\{(C_6H_6)RuTa_6O_{18}\}_2(\mu\text{-}O)]^{10-}$ (**10**$^{10-}$) anion (see scheme 1) built from two fragments

$\{(C_6H_6)RuTa_6O_{18}\}$ joined via a common linear μ_2-O bridge. The formation of $[\{(C_6H_6)RuTa_6O_{18}\}_2(\mu\text{-}O)]^{10-}$ can be viewed as coordination-induced condensation of two hexatantalates according to the equilibrium:

$$[\{(C_6H_6)Ru\}Ta_6O_{19}]^{6-} + H_2O = [\{(C_6H_6)Ru\}Ta_6O_{19}H]^{5-} + OH^-$$
$$2[\{(C_6H_6)Ru\}Ta_6O_{19}H]^{5-} = [\{(C_6H_6)RuTa_6O_{18}\}_2(\mu\text{-}O)]^{10-} + H_2O \quad (1)$$

It is worth stressing that such condensation is unknown for free, non-coordinated hexatantalate. Perhaps, the reduced charge of the 1:1 complex $[\{(C_6H_6)Ru\}Ta_6O_{19}]^{6-}$ facilitates interaction between two negatively charged species; coordination of electron-accepting fragment $\{(C_6H_6)Ru\}^{2+}$ may affect electronic density on the oxygen atoms of the POM part as well.

Decreasing the POM/Ru ratio to 1:2 leads to the bis-capped complex *trans*-$[\{(C_6H_6)Ru\}_2Ta_6O_{19}]^{4-}$ (**11**), isolated as $Na_4[\{(C_6H_6)Ru\}_2Ta_6O_{19}]\cdot 20H_2O$ (Na_4([11]$\cdot 20H_2O$) in high yield. The ESI(−) mass spectrum displays the signal from the triply protonated $[\{(C_6H_6)Ru\}_2Ta_6O_{19} + 3H]^-$ anion (*m/z* 1751.5) as the main peak, accompanied by a minor signal from the doubly protonated $[\{(C_6H_6)Ru\}_2Ta_6O_{19} + 2H]^{2-}$ dianion (*m/z* 875.3). A small amount of monocapped $[\{(C_6H_6)Ru\}Ta_6O_{19} + 5H]^-$ species coexists with the $[\{(C_6H_6)Ru\}_2Ta_6O_{19}]^{4-}$ anion, thus suggesting a plausible dynamic equilibrium between mono- and bis-capped species. The relationship between the Ru/Ta species is summarized in Scheme 1:

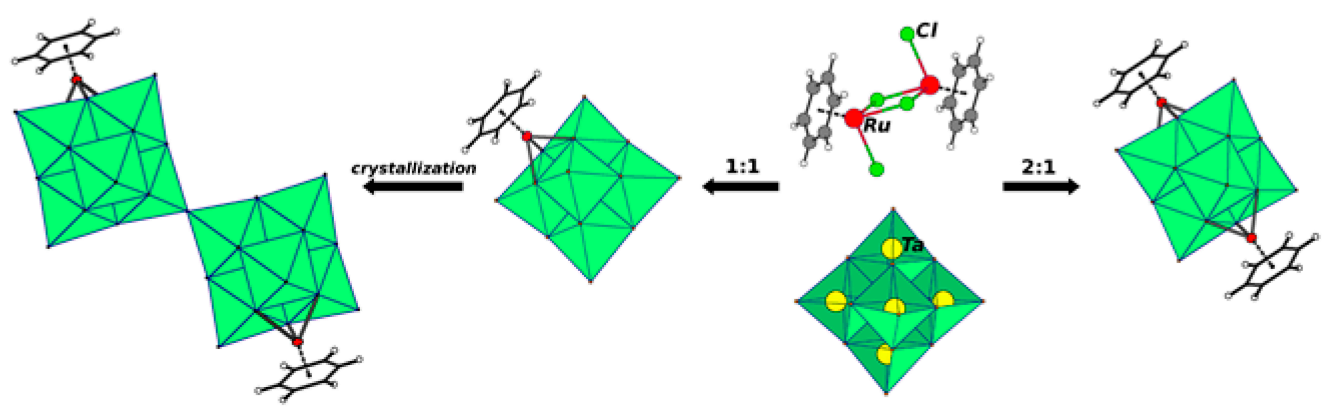

Scheme 1. Formation of 1:1 and 1:2 complexes from $[Ta_6O_{19}]^{8-}$ and $[(C_6H_6)RuCl_2]_2$.

2.3. Reaction $[Nb_6O_{19}]^{8-}$ and Pt^{4+}

Hydrothermal reaction (150 °C) of $[Pt(OH)_4(H_2O)_2]$ with $K_7H[Nb_6O_{19}]\cdot 13H_2O$ in 1:1 molar ratio gives a yellow solution, which shows only one signal in ^{195}Pt NMR spectrum at 3189 ppm. Evaporation of this solution yields yellow crystals of $Cs_2K_{10}[Nb_6O_{19}\{Pt(OH)_2\}]_2\cdot 13H_2O$ (**Cs_2K_{10}-12**). Compound **Cs_2K_{10}-12** was characterized by X-ray structural analysis (see Figure 4 left) [49].

Platinum niobate **12** is a unique dimeric complex, unprecedented in the PONb chemistry, and consists of two Pt(IV) centers coordinated each by three oxygen atoms from a $\{Nb_3O_3\}$ face of a hexaniobate ($d(Pt\text{-}O)_{av}$ 2.028(13), 2.010(14), and 2.124(14) Å), a terminal oxygen of the adjacent $[Nb_6O_{19}]^{8-}$ anion (d(Pt-O) 1.998(11) Å), and bearing two terminal OH groups (d(Pt-O) = 2.015(16) and 1.994(14) Å). Freshly prepared aqueous solution of **12** gives ^{195}Pt NMR spectrum with only one signal at 3189 ppm, the same as is observed in the mother liquor. The negative ESI mass spectrum also strongly suggests that the integrity of the dimeric $[Nb_6O_{19}\{Pt(OH)_2\}]_2^{12-}$ polyanion is preserved in solution.

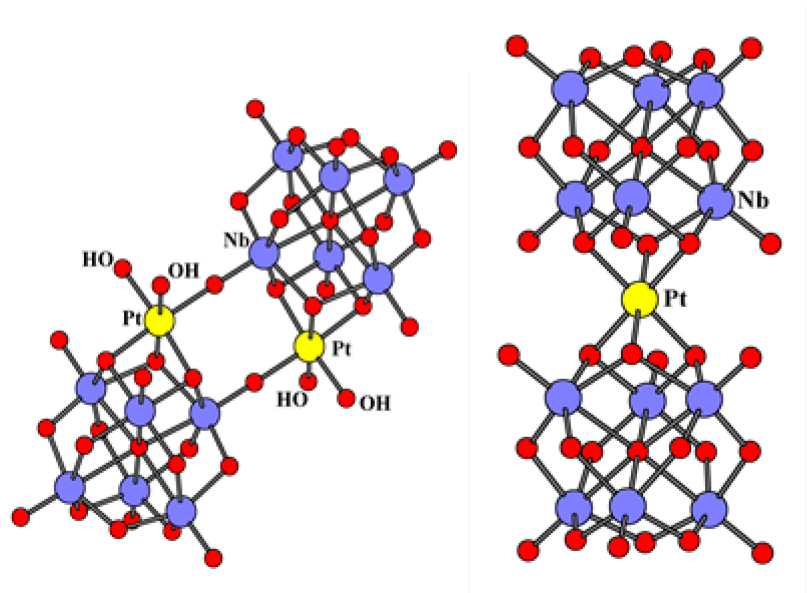

Figure 4. Structure of $[Nb_6O_{19}\{Pt(OH)_2\}]_2^{12-}$ (**12**$^{12-}$) (left) and structure of $[Pt(Nb_6O_{19})_2]^{12-}$(**13**$^{12-}$) (right), ball and stick models.

Reaction of $[Pt(OH)_4(H_2O)_2]$ and $K_7H[Nb_6O_{19}]\cdot 13H_2O$ in the 1:2 molar ratio at 160–190 °C gives a yellow solution, which has two ^{195}Pt NMR signals at 3189 and 3422 ppm with relative intensities 0.75/0.25. Slow evaporation of this solution in a glass beaker produces light-yellow crystals of $Na_2K_{10}[Pt(Nb_6O_{19})_2]\cdot 18H_2O$ (**Na_2K_{10}-13)** in 20% yield (Na^+ comes from glass leaching). The sandwich-type anion $[Pt(Nb_6O_{19})_2]^{12-}$ (**13**$^{12-}$) is a new (fourth) member of the well-known $[M(Nb_6O_{19})_2]^{n+}$ (M = Mn, Ni, Co) family (Figure 4 right). All the Pt-O distances are equivalent, being 2.042(1) Å. The salt **Na_2K_{10}-13** is isotypic with $K_6Na_2[Co^{III}H_5(Nb_6O_{19})_2]\cdot 26.5H_2O$ [30].

Further evaporation of the solution gives **Cs_2K_{10}-12**. A freshly prepared solution of **Na_2K_{10}-13** demonstrates only one, slightly broadened, signal at 3422 ppm. Aged solutions give rise to increasingly intense signal at 3189 ppm, corresponding to the formation of $[Nb_6O_{19}\{Pt(OH)_2\}]_2^{12-}$ (**12**). This observation implies a dynamics in solution, where $[Pt(Nb_6O_{19})_2]^{12-}$ (**13**) slowly converts into $[Nb_6O_{19}\{Pt(OH)_2\}]_2^{12-}$ (**12**). Taking advantage of the versatility and high sensitivity of the ESI-MS technique for tracing solution speciation in the POM chemistry [47,50], we recorded ESI-MS spectrum of aqueous solution of **Cs_2K_{10}-12** equilibrated for one week. ESI-MS results suggest coexistence of at least four different species in solution. Beside **12** and **13**, the ESI-MS data suggest the presence of free Lindqvist $[Nb_6O_{19}]^{8-}$ polyanion and a species that corresponds to the $[Nb_6O_{19}Pt(OH)_3]^{7-}$ anion whose structure might putatively correspond to capping of $[Nb_6O_{19}]^{8-}$ with a $\{Pt(OH)_3\}^+$ group. Remarkably, the platinum niobate **Cs_2K_{10}-12** exhibits electrocatalytic activity for water oxidation in 0.1 M Na_2SO_4. Oxidation process generates a significant rise in the current for a catalytic process mediated by the complex. The current in the presence of the platinum niobate is several times higher than for the blank solution. This electrochemical behavior is similar to the reported for the nonatungstate complex with a tetrarhodium-oxo core [51].

3. Reactivity of Heteropolyniobates towards Noble Metal Complexes

In 1979, S.K. Ray reported that reaction of $K_7H[Nb_6O_{19}]\cdot 13H_2O$ with H_6TeO_6 gave a heteropolyniobate formulated as $K_8H_2[TeNb_{12}O_{38}]\cdot 13H_2O$ [52]. This formula was deduced uniquely from elemental analysis. Such stoichiometry could imply that this compound would be analogous with the known heteropolyniobates $[(Nb_6O_{19})_2M]^{n-}$ (M = Co, Ni, Mn, Pt) with octahedral Te^{VI} sandwiched between two hexaniobates. We were curious if it were really so and repeated these experiments, only to find out that the purported "dodecaniobate" was in fact $[(OH)TeNb_5O_{18}]^{6-}$, which can be regarded simply as a substituted hexaniobate with one $\{NbO\}^{3+}$ vertex replaced with a $\{TeOH\}^{5+}$ vertex. In fact, this complex had been already identified by W. Casey and co-workers, who prepared it from $Nb_2O_5\cdot xH_2O$, Me_4NOH and H_6TeO_6 in methanolic solution [53]. Perhaps, the authors of [52] dealt with an approximately stoichiometric mixture of $[(OH)TeNb_5O_{18}]^{6-}$ and $[Nb_6O_{19}]^{8-}$, which led them to the wrong conclusion about the composition of the product. Surface charge density of telluroniobate is lower than in the hexaniobate, which means that their reactivity might be different. In order to check the significance of this difference, reactivity studies towards noble metal complexes have been extended in our group to the telluroniobate $[(OH)TeNb_5O_{19}]^{6-}$.

3.1. Reaction $[(OH)TeNb_5O_{19}]^{6-}$ with $\{Cp^*Rh\}^{2+}$ and $\{Cp^*Ir\}^{2+}$

We investigated reaction of $[(OH)TeNb_5O_{18}]^{6-}$ with $[Cp^*MCl_2]_2$ as sources of $\{Cp^*M\}^{2+}$ (M = Rh, Ir). Despite the difference in the surface charge density between $[(OH)TeNb_5O_{18}]^{6-}$ and $[Nb_6O_{19}]^{8-}$, formation of double-capped complexes takes place as easily as with hexaniobate. Crystal structure of $Na_2[\{Cp^*Rh\}_2Te(OH)Nb_5O_{18}]\cdot 24H_2O$ (**14**) shows coordination of two $\{Cp^*Rh\}^{2+}$ fragments, with the Te atom localized in the central M_4 plane of Lindqvist-type anion as illustrated in Figure 5. Two other metal positions are fully occupied by niobium. However, this disorder corresponds to four different orientations of a *single* isomer which is the only possible structure for the *trans* complex in the solid state.

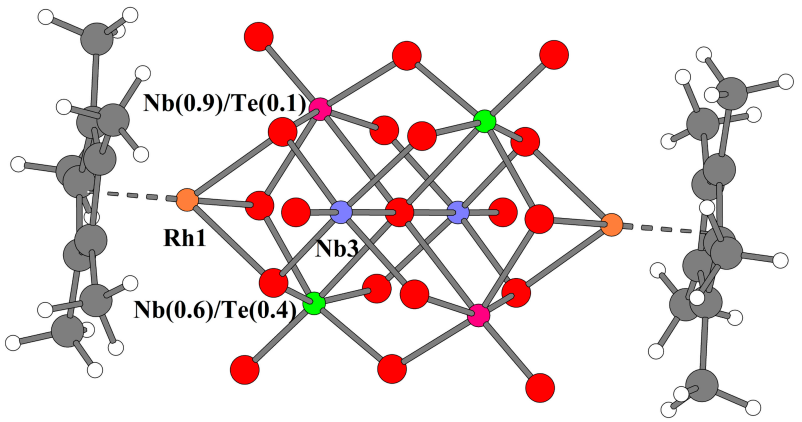

Figure 5. Structure of $[\{Cp^*Rh\}_2Te(OH)Nb_5O_{19}]^{2-}$ anion (**14**), positions of Te atom with different occupancies are colored in green and purple (ball and stick model).

3.2. Reaction $[(OH)TeNb_5O_{19}]^{6-}$ with $\{(C_6H_6)Ru\}^{2+}$

Reactivity studies on $[(OH)TeNb_5O_{18}]^{6-}$ were also extended to $[(C_6H_6)RuCl_2]_2$ as source of the $\{(C_6H_6)Ru\}^{2+}$. ESI-MS can be conveniently used to monitor the advance of the reaction. Grafting of one and two $\{(C_6H_6)Ru\}^{2+}$ fragments can be immediately inferred from the characteristic *m/z* shifts to higher values, as illustrated in Figure 6. Moreover, the uptake of one or two Ru-containing fragments confers a new characteristic isotopic pattern due to multiple isotopes of the Ru at the natural abundance. Formation of single and double capped complexes $[(OH)TeNb_5O_{18}\{(C_6H_6)Ru\}]^{4-}$ (**15**) and $[(OH)TeNb_5O_{18}\{(C_6H_6)Ru\}_2]^{2-}$ (**16**) takes place as smoothly as with hexaniobate. Characteristic peaks at *m/z* 539.1 and 628.1 correspond to formulations $[(OH)TeNb_5O_{18}\{(C_6H_6)Ru\} + 2H]^{2-}$ and $[(OH)TeNb_5O_{18}\{(C_6H_6)Ru\}_2]^{2-}$, respectively. Other species based upon **15** and **16** associated Na^+ or K^+ adducts are also evident.

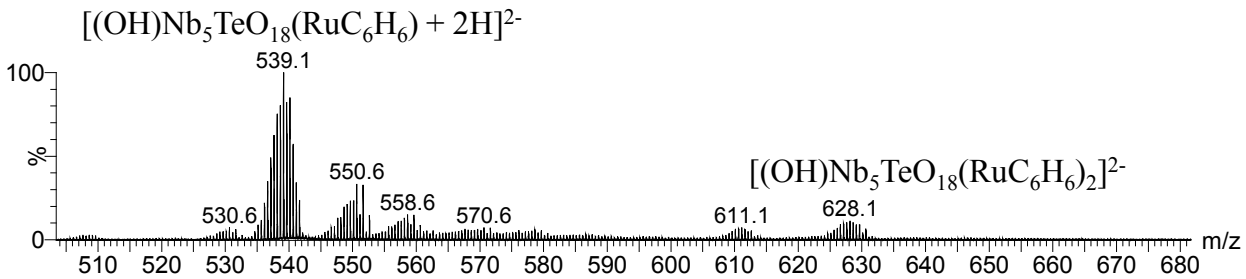

Figure 6. ESI mass spectrum of the reaction mixture between $[(OH)Nb_5O_{18}]^{6-}$ and $[(C_6H_6)RuCl_2]_2$ with POM / Ru ratio 1:1.

3.3. Reaction $[SiNb_{12}O_{40}]^{16-}$ with $\{(C_6H_6)Ru\}^{2+}$

Studies on the complexation with the siliconiobate $[SiNb_{12}O_{40}]^{16-}$ [54] are particularly relevant. Because of its high negative charge, it is expected to be much more "sticky" than well-known Group 6 Keggin complexes $[EM_{12}O_{40}]^{n-}$ (n = 2–6) (M = Mo, W) which are often regarded as non-coordinating [55]. It can be anticipated that quite a large number of metal fragments could be grafted to $[SiNb_{12}O_{40}]^{16-}$. Following this rationale, we undertook preliminary exploration of the reaction of $[SiNb_{12}O_{40}]^{16-}$ with $[(C_6H_6)RuCl_2]_2$, and ESI-MS results indicate that up to four $\{(C_6H_6)Ru\}^{2+}$ fragments can be grafted to $[SiNb_{12}O_{40}]^{16-}$, leading to the species formulated as $[\{(C_6H_6)Ru\}_4SiNb_{12}O_{40}]^{8-}$ (**17**).

4. Analytical Tools to Study Solution Speciation in Nb and Ta POM Chemistry

One of the general features of the reactivity of POMs is their lability in aqueous solutions up to the point that such solutions can be regarded as virtual libraries of different building blocks, which equilibrate together and can form different structures depending on counter cations, pH and *etc.* The simplest case is protonation. The hexametalate anions $[M_6O_{19}]^{8-}$ (M = Nb, Ta) are very basic. For example, hexaniobate in water exists as $[H_3Nb_6O_{19}]^{5-}$ (pH = 8), $[H_2Nb_6O_{19}]^{6-}$ (pH = 10), $[HNb_6O_{19}]^{7-}$ (pH = 12), and $[Nb_6O_{19}]^{8-}$ (pH = 14) [56]. Similarly, for hexatantalate three protonated species, $[HTa_6O_{19}]^{7-}$, $[H_2Ta_6O_{19}]^{6-}$, and $[H_3Ta_6O_{19}]^{5-}$ were found [57–59]. Even in aqueous NBu_4OH hexatantalate exists as $[H_2Ta_6O_{19}]^{6-}$ [60]. Small-angle X-ray scattering (SAXS) studies of $[Ta_6O_{19}]^{8-}$

and $[Nb_6O_{19}]^{8-}$ in water have been reported and important differences in the solution behavior have been observed due to the distinctive propensity to aggregation with counteractions for M = Ta and Nb [61]. Uv-vis spectroscopy complemented with DFT calculations have been also reported [62]. More complicated processes connected with rearrangement of POM backbone can take place [63–65]. It is obvious that proving the identity between species existing in solid state and solution is a very important part of this chemistry. However, the study of solution behavior of polyniobates and polytantalates is a challenging task. These species are colorless, diamagnetic, show no redox behavior and are, under most conditions, in a dynamic equilibrium. In this section, useful analytical tools that can provide complementary signatures for the Nb and Ta POM characterization in solution are discussed. In particular, the usefulness of ^{1}H NMR, ^{1}H NMR Diffusion Ordered Spectroscopy (DOSY), capillary electrophoresis and ESI-MS in concert is underlined. An illustrative example is given to demonstrate the complementarily of all techniques to determine stoichiometry and solution dynamics.

The possibilities of NMR are restricted to the use of ^{17}O, which unfortunately has very low natural abundance and sensitivity. It was used, for example, to follow the conversion of several niobates in water [66,67]. However, coordination of organometallic fragments to niobates and tantalates provides new opportunities for use of NMR for solution studies. In particular, structural information can be gained from ^{1}H NMR signals of the organic ligands attached to the grafted heterometal, which would tell us about the overall symmetry of the compound. Moreover, it is possible to estimate diffusion coefficients from ^{1}H NMR DOSY of the organic part that can be subsequently used to calculate molecular weight of a particular species. This ^{1}H DOSY NMR technique is becoming a powerful tool for the determination of the size (hydrodynamic radius) and the molecular weight of inorganic clusters [68–70]. This technique has not been virtually used in the chemistry of Nb and Ta POM prior to our work.

Another useful tool for solution studies is capillary electrophoresis (CE). It is rarely used in the chemistry of POMs [71,72]. The possibilities opened up by the use of CE for POMs mixtures were studied in a few cases [73]. Although in these works CE revealed itself as a promising analytical tool, its potential for POM chemistry is far from being fully exploited. Combination of CE, HPLC and other methods (in particular ESI-MS and NMR) can provide sufficient information about quantitative and qualitative composition of solutions, numbers of POM species, and their stability and evolution with time.

Accurate determination of the formulae and structure of new compounds remains an important issue in POM chemistry. In this respect, use of soft ionization mass spectrometric techniques, and in particular, ESI techniques, is becoming widespread. Excellent reviews on the use of soft ionization MS techniques can be found elsewhere; for example, Cronin *et al.* illustrated the versatility of ESI and cryospray ionization techniques not only for characterization of final POM assemblies, but also to prove mechanisms of self-assembly of supramolecular POM-based architectures in solution [47,50]. Ohlin *et al.* reported an important work on this topic highlighting different approaches to obtain reliable information on the dynamic solution of POM on the basis of ESI-MS [47]. However, there are several potential limitations to using ESI-MS alone for the investigation of POM. This is the case when dynamic speciation involving hydroxy-bridged POM species, the pH value, ionic strength or the counteraction plays an important role. In addition, during the ESI process itself, the samples undergo dramatic changes in pH and concentration, which may perturb the speciation equilibrium. Moreover, due to the high charge state and molecular weight, the use of ESI-MS spectrometers equipped with high resolution analysers is important to facilitate unambiguous molecular compositions'

determination. In this part, we will discuss a case study, where we used ESI-MS, ^{1}H DOSY NMR and CE techniques, combined together, in order to elucidate the solution behavior of the $\{(C_6H_6)Ru\}^{2+}/[Ta_6O_{19}]^{8-}$ system to afford compounds **9** and **10** [48].

4.1. $\{(C_6H_6)Ru\}^{2+}/[Ta_6O_{19}]^{8-}$ System—Case Study

The ^{1}H DOSY NMR experiment performed on a sample of $Na_{10}[10]\cdot 39.4H_2O$ in D_2O (see Figure 7) yielded the self-diffusion coefficients D = 315 ± 10 μm²·s^{-1} and D = 325 ± 10 μm²·s^{-1}, respectively, for the ^{1}H NMR signals located at 5.85 ppm and 5.94 ppm. The Stokes-Einstein relation $D=\frac{kT}{6\pi\eta R_H}$ (which describes the diffusion coefficient D for spherical objects, where k is the Boltzmann constant, T the temperature taken equal to 300 K in this study, η of the solvent viscosity taken equal to that of water at 300 K (1.002 Pa.s) and R_H the hydrodynamic radius) gave hydrodynamic radii of 6.75–6.96 Å which are compatible with the radii expected for *solvated monomeric* species $[\{(C_6H_6)Ru\}Ta_6O_{19}]^{6-}$ and $[\{(C_6H_6)Ru\}_2Ta_6O_{19}]^{4-}$ but *not with the dimeric* $[\{(C_6H_6)RuTa_6O_{18}\}_2(\mu\text{-}O)]^{10-}$.

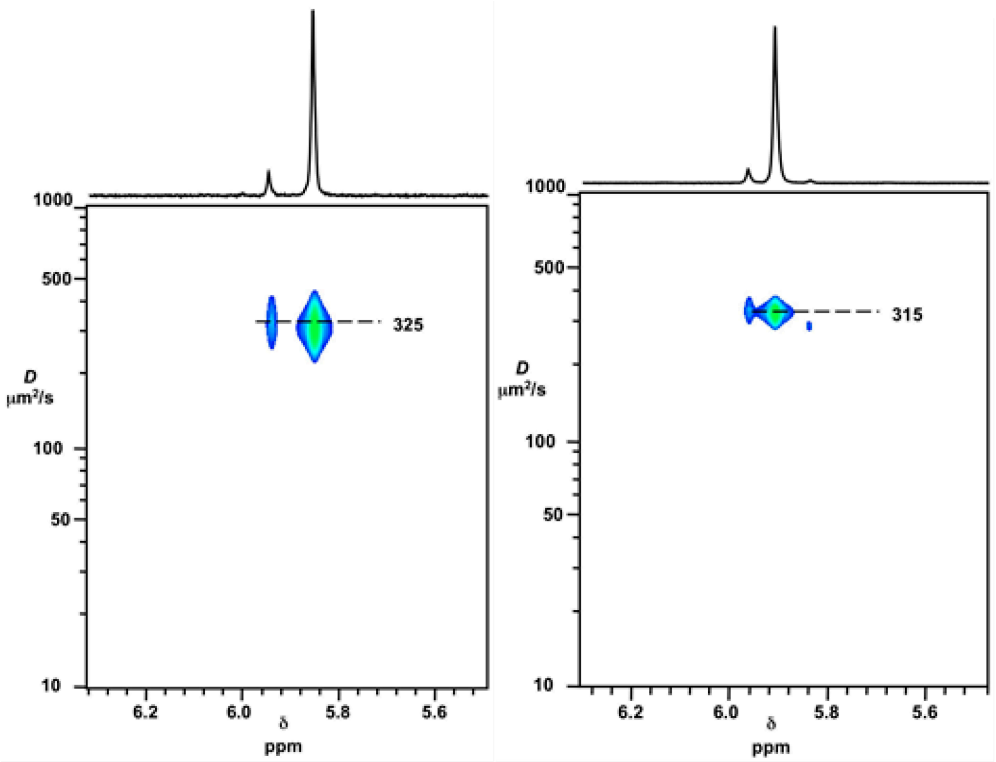

Figure 7. ^{1}H DOSY NMR spectra of **Na_{10}-10** in D_2O (**left**) and ^{1}H DOSY NMR spectra of **Na_4-9** in D_2O (**right**).

The ^{13}C NMR spectrum of $Na_4[\{(C_6H_6)Ru\}_2Ta_6O_{19}]\cdot 20H_2O$ (**Na_4-9**) in D_2O exhibits two signals at 81.95 ppm and 81.82 ppm, with the complementary set of signals in the ^{1}H NMR spectrum at 5.97 (6%) ppm and 5.92 (93%) ppm and 5.85 (≤1%). This pattern corresponds to a mixture of *cis* (6%) and *trans* (93%) isomers of $[\{(C_6H_6)Ru\}_2Ta_6O_{19}]^{4-}$, similarly to what was observed for $[\{(p\text{-cymene})Ru\}_2Nb_6O_{19}]^{4-}$[6], while the minor peak at 5.85 ppm is to be attributed to the 1:1 complex $[\{(C_6H_6)Ru\}Ta_6O_{19}]^{6-}$. The ^{1}H DOSY NMR experiment gives the self-diffusion coefficients D = 315 ±

10 μm² s^{-1} and D = 325 ± 10 μm² s^{-1} for the signals at 5.92 and 5.97 ppm, respectively, whereas the low intensity of the minor peak has prevented accurate determination of the D value. These values correspond to hydrodynamic radii in the 0.675–0.696 nm range. This is identical to that obtained for the solutions of $Na_{10}[\{(C_6H_6)RuTa_6O_{18}\}_2(\mu\text{-}O)]\cdot 39.4H_2O$ and agree well with the attribution of ^1H NMR peaks to *cis*-$[\{(C_6H_6)Ru\}_2Ta_6O_{19}]^{4-}$ (5.97 ppm), *trans*-$[\{(C_6H_6)Ru\}_2Ta_6O_{19}]^{4-}$ (5.92 ppm), and $[\{(C_6H_6)Ru\}Ta_6O_{19}]^{6-}$ (5.85 ppm). These results necessarily imply two equilibria. The first corresponds to *cis-trans* isomerization process, strongly displaced towards the *trans* isomer. The latter corresponds to the de-coordination of a $\{(C_6H_6)Ru\}^{2+}$ moiety. This hypothesis is supported by the observation of a small broad peak at 5.4 ppm, attributed to $[(C_6H_6)_2Ru_2(OH)_3]^+$ (see Equation 2).

$$\begin{gathered} \textit{trans}\text{-}[\{(C_6H_6)Ru\}_2Ta_6O_{19}]^{4-} = \textit{cis}\text{-}[\{(C_6H_6)Ru\}_2Ta_6O_{19}]^{4-} \\ 2[\{(C_6H_6)Ru\}_2Ta_6O_{19}]^{4-} + 3OH^- + = 2[\{(C_6H_6)Ru\}Ta_6O_{19}]^{6-} + [(C_6H_6)_2Ru_2(\mu\text{-}OH)_3]^+ \end{gathered} \quad (2)$$

ESI(−) mass analysis of Na_{10}-**10** in water reveals only the presence of the *monomeric* $\mathbf{9}^{6-}$ species, thus indicating that the dimerization depicted in Eq. 1 is a reversible process ongoing from the solution to the solid state and *vice versa*. The electrophorograms recorded for aqueous solutions of $\mathbf{Na_{10}}$**-10** and $\mathbf{Na_4}$**-9** are presented in Figure 8. The solutions of $\mathbf{Na_{10}}$**-10**, to which some amount of $\mathbf{Na_4}$**-9** has been added as reference, give two well-resolved peaks (Figure 7). The second peak corresponds to **9**, which was confirmed by UV-spectroscopy and by the standard addition method. The first peak must therefore correspond to the *monomeric* $[\{(C_6H_6)Ru\}Ta_6O_{19}]^{6-}$ species (or its dominant protonated form), because the signal from the dimer with its larger size and charge, should appear after the signal of **10**, and with a longer retention time. Thus, combination of ESI-MS and CE gives coherent evidence that in aqueous solutions $[\{(C_6H_6)RuTa_6O_{18}\}_2(\mu\text{-}O)]^{10-}$ *dissociates into the monomeric* $[\{(C_6H_6)Ru\}Ta_6O_{19}]^{6-}$.

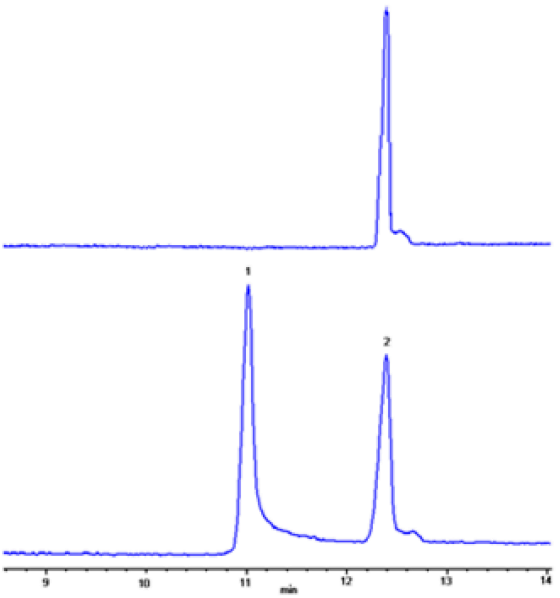

Figure 8. The electrophorogram of complex $\mathbf{Na_4}$**-9** (up). The electrophorogram of complex $\mathbf{Na_{10}}$**-10** solution with addition of complex $\mathbf{Na_4}$**-9** as reference (down). Fused-silica capillary 50μm i.d. × 75 sm; sample buffer: $7.5\cdot 10^{-3}$M borate (pH 9.18); running buffer: $7{,}5\cdot 10^{-2}$ M borate (pH 9.18).

5. Conclusions

The chemistry of niobium and tantalum polyoxoanions still belongs to a little researched area of inorganic chemistry. Many unusual complexes still remain hidden, and isolation of principally new $[(Ta_6O_{18})_2(\mu\text{-}O)]^{14-}$ backbone is a tantalyzing hint at this potential richness. In this short review, we summarized our recent research focused on the coordination of noble metals to hexametalates. Grafting of $\{Cp^*M\}^{2+}$ (M = Rh, Ir) on the surface of Lindqvist-type hexametalates (including $[(OH)TeNb_5O_{19}]^{6-}$) was studied with full characterization of the hybrid complexes in solid state and solution. Coordination of $\{(C_6H_6)Ru\}^{2+}$ to $[Ta_6O_{19}]^{8-}$ gives unprecedented $[(\{(C_6H_6)Ru\}Ta_6O_{18})_2(\mu\text{-}O)]^{10-}$. Complexation of Pt(IV) with $[Nb_6O_{19}]^{8-}$ was studied with different techniques. New dimeric complex $[(Nb_6O_{19}\{Pt(OH)_2\})_2]^{12-}$ is obtained when hexaniobate reacts with Pt(IV) in 1:1 molar ratio, while increasing the Pt/Nb_6 ratio to 2:1 gives sandwich-type complex $[Pt(Nb_6O_{19})_2]^{12-}$. We used different, both traditional and non-traditional, analytical tools for studying the solution behavior of individual reaction products and reaction mixtures, a challenging task for the systems where few analytical methods are readily available. The ^1H, ^{13}C and DOSY NMR techniques combined with ESI-MS and CE highlight are adequate tools for characterization of complex solutions. An illustrative example dealing with the $\{(C_6H_6)Ru\}^{2+}/[Ta_6O_{19}]^{8-}$ system demonstrates complementarity of all these techniques for determination of stoichiometry and solution dynamics, an approach both promising and highly recommendable to trace unambiguously the identity of large inorganic systems [74].

Acknowledgments

Authors thanks SCIC of the UJI and all members of our Russian-Spanish-French team for very fruitful collaboration. This work was supported by Russian Scientific Foundation (RScF 14-13-00645).

Author Contributions

The manuscript was written with equal contributions from all authors. MNS owns the general idea and plan of the publication, and he wrote parts 1 and 3, as well as Conclusions. PAA authored part 2, and CV was the main contributor to part 4.

Conflicts of Interest

The authors declare no conflict of interest.

References

1. Livage, J. Synthesis of polyoxovanadates via “chimie douce”. *Coord. Chem. Rev.* **1998**, *178–180*, 999–1018.
2. Hayashi, Y. Hetero and lacunary polyoxovanadate chemistry: Synthesis, reactivity and structural aspects. *Coord. Chem. Rev*. **2011**, *255*, 2270–2280.

3. Müller, A.; Sessoli, R.; Krickemeyer, E.; Bögge, H.; Meyer, J.; Gatteschi, D.; Pardi, L.; Westphal, J.; Hovemeier, K.; Rohlfing, R.; *et al.* Polyoxovanadates: High-Nuclearity Spin Clusters with Interesting Host–Guest Systems and Different Electron Populations. Synthesis, Spin Organization, Magnetochemistry, and Spectroscopic Studies. *Inorg. Chem.* **1997**, *36*, 5239–5250.
4. Breen, J.M.; Zhang, L.; Clement, R.; Schmitt, W. Hybrid Polyoxovanadates: Anion-Influenced Formation of Nanoscopic Cages and Supramolecular Assemblies of Asymmetric Clusters. *Inorg. Chem.* **2012**, *51*, 19–21.
5. Zhang, L.; Schmitt, W. From Platonic Templates to Archimedean Solids: Successive Construction of Nanoscopic $\{V_{16}As_8\}$, $\{V_{16}As_{10}\}$, $\{V_{20}As_8\}$, and $\{V_{24}As_8\}$ Polyoxovanadate Cages. *J. Am. Chem. Soc.* **2011**, *133*, 11240–11248.
6. Gatteschi, D.; Sessoli, R.; Müller, A.; Kögerler, P. Polyoxometalate chemistry: A source for unusual spin topologies. In *Polyoxometalate Chemistry*; Pope, M.T., Müller, A., Eds.; Kluwer: Dordrecht, The Netherlands, 2001; p. 319;
7. Choi, J.; Sanderson, L.A.W.; Musfeldt, J.L.; Ellern, A.; Kögerler, P. Optical properties of the molecule-based magnet $K_6[V_{15}As_6O_{42}(H_2O)]\cdot 8H_2O$. *Phys. Rev. B* **2003**, *68*, 064412;
8. Gatteschi, D.; Pardi, L.; Barra, A.L.; Müller, A. Polyoxovanadates: The Missing Link between Simple Paramagnets and Bulk Magnets? *Mol. Eng.* **1993**, *3*, 157–169.
9. Nymann, M. Polyoxoniobate chemistry in the 21st century. *Dalton Trans.* **2011**, *40*, 8049–8058.
10. Kato, R.; Kobayashi, A.; Sasaki, Yu. 1:14 Heteropolyvanadate of phosphorus: preparation and structure. *J. Am. Chem. Soc.* **1980**, *102*, 6571–6572.
11. Kato, R.; Kobayashi A.; Sasaki, Yu. The heteropolyvanadate of phosphorus. Crystallographic and NMR studies. *Inorg. Chem.* **1982**, *21*, 240–246.
12. Nomiya, K.; Kato, K.; Miwa, M. Preparation and spectrochemical properties of soluble vanadophosphate polyanions with bicapped-Keggin structure. *Polyhedron* **1986**, *5*, 811–813.
13. Khan, M.I.; Zubieta, J.; Toscano, P. Protonation sites in a heteropolyvanadate of phosphorus: X-ray crystal structure of $(Me_3NH)_4(NH_4)[H_4PV_{14}O_{42}]$. *Inorg. Chim. Acta* **1992**, *193*, 17–20.
14. Nakamura, S.; Yamawaki, T.; Kusaka, K.; Otsuka, T.; Ozeki, T. Hydrogen-bond Networks Involving Protonated Bicapped-Keggin Tetradecavanadophosphate Anions. *J. Clust. Sci.* **2006**, *17*, 245–256.
15. Grabau, M.; Forster, J.; Heussner, K.; Streb, C. Synthesis and Theoretical Hirshfeld Analysis of a Supramolecular Heteropolyoxovanadate Architecture. *Eur. J. Inorg. Chem.* **2011**, 1719–1724.
16. Fang, X.; Kögerler, P.; Speldrich, M.; Schilder, H.; Luban, M. A polyoxometalate-based single-molecule magnet with an $S = 21/2$ ground state. *Chem. Commun.* **2012**, *48*, 1218–1220.
17. Monakhov, K.Yu.; Linnenberg, O.; Kozłowski, P.; van Leusen, J.; Besson, C.; Secker, T.; Ellern, A.; López, X.; Poblet, J.M.; Kögerler, P. Supramolecular Recognition Influences Magnetism in $[X@HV^{IV}_8V^{V}_{14}O_{54}]^{6-}$ Self-Assemblies with Symmetry-Breaking Guest Anions. *Chem. Eur. J.* **2015**, *21*, 2387–2397.
18. Dale, B.W.; Pope, M.T. The heteropoly-12-niobomanganate(IV) anion. *J. Chem. Soc. Chem. Commun*. **1967**, 792–792.
19. Flynn, C.M., Jr.; Stucky, G.D. Heteropolyniobate complexes of manganese(IV) and nickel(IV). *Inorg. Chem*. **1969**, *8*, 332–334.

20. Flynn, C.M., Jr.; Stucky, G.D. Crystal structure of sodium 12-niobomanganate(IV),$Na_{12}MnNb_{12}O_{38}\cdot 50H_2O$. *Inorg. Chem.* **1969**, *8*, 335–344.
21. Kheddar, N.; Spinner, B. Constitution et domaines de stabilite des oxaloniobates en solution aqueuse. *Bull. Soc. Chim. Fr.* **1972**, *2*, 502–506 (In French).
22. Marty, A.; Abdmeziem, K.; Spinner, B. Une nouvelle condensation pour des sels du niobium V: les nonaniobates de tetramethyl et de tetraethylammonium. *Comptes Rendus C.* **1976**, *283*, 285–288.
23. Marty, A.; Abdmeziem, K.; Spinner, B. De noveaux isopolyanions du niobium V: comportement en solution aqueuse des nonaniobates de tetramethyl et tetraethylammonium. *Bull. Soc. Chim. Fr.* **1977**, *3–4*: 231–238 (In French).
24. Goiffon, A.; Philippot, E.; Maurin, M. Structure cristalline du niobate 7/6 de sodium $(Na_7)(H_3O)Nb_6O_{19}\cdot 14H_2O$. *Rev. Chim. Miner*. **1980**, *17*, 466–476
25. Graeber, E.J.; Morosin, B. The molecular configuration of the decaniobate ion ($Nb_{10}O_{28}^{6-}$) *Acta Cryst.* **1977**, *33*, 2137–2143.
26. Villa, E.M.; Ohlin, C.A.; Balogh, E.; Anderson, T.M.; Nyman, M.D.; Casey, W.H. Reaction Dynamics of the Decaniobate Ion $[H_xNb_{10}O_{28}]^{(6-x)-}$ in Water. *Angew. Chem. Int. Ed.* **2008**, *47*, 4844–4846.
27. Matsumoto, M.; Ozawa, Y.; Yagasaki, A.; Zhe, Y. Decatantalate—The Last Member of the Group 5 Decametalate Family. *Inorg. Chem.* **2013**, *52*, 7825–7827.
28. Hayashi, Y.; Ozawa, Y.; Isobe, K. The first vanadate hexamer capped by 4 cyclopentadienyl-rhodium or cyclopentadienyl-iridium groups. *Chem. Lett.* **1989**, 425–428.
29. Chae, H.K.; Klemperer, W.G.; Day, V.W. Organometal hydroxide route to $[(C_5Me_5)Rh]_4(V_6O_{19})$ *Inorg. Chem*. **1989**, *28*, 1423–1424.
30. Ma, P.T.; Chen, G.; Wang, G.; Wang, J.P. Cobalt—Sandwiched lindqvist hexaniobate dimer $[Co(III)H_5(Nb_6O_{19})_2]^{8-}$. *Rus. J. Coord. Chem.* **2011**, *37*, 772–775.
31. Antonio, M.R.; Nyman, M.; Anderson, T. M. Direct Observation of Contact Ion-Pair Formation in Aqueous Solution. *Angew. Chem. Int. Ed*. **2009**, *48*, 6136–6140.
32. Dale, B.W.; Buckley, J.M.; Pope, M.T. Heteropoly-niobates and -tantalates containing manganese(IV). *J. Chem. Soc. A.* **1969**, 301–304.
33. Flynn, C.M., Jr.; Stucky, G.D. Sodium 6-niobo(ethylenediamine)cobaltate(III) and its chromate(III) analog. *Inorg. Chem*. **1969**, *8*, 178–180.
34. Bontchev, R.P.; Nyman, M. Evolution of Polyoxoniobate Cluster Anions. *Angew. Chem., Int. Ed.*, **2006**, *45*,6670–6672.
35. Niu, J.Y.; Ma, P.T.; Niu, H.Y.; Li, J.; Zhao, J.W.; Song, Y.; Wang, J.P. Giant Polyniobate Clusters Based on $[Nb_7O_{22}]^{9-}$ Units Derived from a Nb_6O_{19} Precursor. *Chem.–Eur. J.*, **2007**, *13*, 8739–8748.
36. Chen, G.; Ma, P.T.; Wang, J.P.; Niu, J.Y. A new organic–inorganic hybrid polyoxoniobate based on Lindqvist-type anion and nickel complex. *J. Coord. Chem.* **2010**, *63*, 3753–3763.
37. Hegetschweiler, K.; Finn, R.C.; Rarig, R.S.; Sander, J.; Steinhauser, S.; Worle, M.; Zubieta, J. Surface complexation of $[Nb_6O_{19}]^{8-}$ with NiII: solvothermal synthesis and X-ray structural characterization of two novel heterometallic Ni-Nb-polyoxometalates. *J. Inorg. Chim. Acta* **2002**, *337*, 39–47.

38. Dickman, M.H.; Pope, M.T. Robust, Alkali-Stable, Triscarbonyl Metal Derivatives of Hexametalate Anions, $[M_6O_{19}\{M'(CO)_3\}_n]^{(8-n)-}$ (M = Nb, Ta; M' = Mn, Re; *n* = 1, 2). *Inorg. Chem.* **2001**, *40*, 2582–2586.
39. Laurencin, D.; Thouvenot, R.; Boubekeur, K.; Proust, A. Synthesis and reactivity of $\{Ru(p\text{-cymene})\}^{2+}$ derivatives of $[Nb_6O_{19}]^{8-}$: A rational approach towards fluxional organometallic derivatives of polyoxometalates. *Dalton Trans.* **2007**, 1334–1345.
40. Hill, C.L.; Prosser-McCartha, C.M. Homogeneous catalysis by transition metal oxygen anion clusters. *Coord. Chem. Rev.* **1995**, *143*, 407–455.
41. Vasilchenko, D.; Tkachev, S.; Baidina, I.; Korenev, S. Speciation of Platinum(IV) in Nitric Acid Solutions. *Inorg. Chem*. **2013**, *52*, 10532–10541.
42. Huang, P.; Qin, C.; Su, Z.-M.; Xing, Y.; Lang, X.-L.; Shao, K.-Z.; Lan, Y.-Q.; Wang, E.-B. Self-Assembly and Photocatalytic Properties of Polyoxoniobates: $\{Nb_{24}O_{72}\}$, $\{Nb_{32}O_{96}\}$, and $\{K_{12}Nb_{96}O_{288}\}$ Clusters. *J. Am. Chem. Soc.* **2012**, *134*, 14004–14010.
43. Lee, U.; Joo, H.C.; Park, K.M.; Mal, S.S.; Kortz, U.; Keita, B.; Nadjo, V. Facile Incorporation of Platinum(IV) into Polyoxometalate Frameworks: Preparation of $[H_2Pt^{IV}V_9O_{28}]^{5-}$ and Characterization by 195Pt NMR Spectroscopy. *Angew. Chem. Int. Ed.* **2008**, *47*, 793–796.
44. Kortz, U.; Lee, U.; Joo, H.C.; Park, K.M.; Mal, S.S.; Dickman, M.H.; Jameson, G.B. Platinum-Containing Polyoxometalates. *Angew. Chem. Int. Ed*. **2008**, *47*, 9383–9384.
45. Abramov, P.A.; Sokolov, M.N.; Virovets, A.V.; Floquet, S.; Haouas, M.; Taulelle, F.; Cadot, E.; Vicent, C.; Fedin, V. Grafting $\{Cp^*Rh\}^{2+}$ on the surface of Nb and Ta Lindqvist-type POM. *Dalton Trans.* **2015**, *44*, 2234–2239.
46. Di Marco, V.B.; Bombi, G.G. Electrospray mass spectrometry (ESI-MS) in the study of metal-ligand solution equilibria. *Mass Spectrom. Rev.* **2006**, *25*, 347–379.
47. Ohlin, C.A. Reaction Dynamics and Solution Chemistry of Polyoxometalates by Electrospray Ionization Mass Spectrometry. *Chem.-Asian J.* **2012**, *7*, 262–270.
48. Abramov, P.A.; Sokolov, M.N.; Floquet, S.; Haouas, V.; Taulelle, V.; Cadot, V.; Peresypkina, E.V.; Virovets, A.V.; Vicent, C.; Kompankov, N.B.; Zhdanov, A.A.; Shuvaeva, O.V.; Fedin, V.P. Coordination-Induced Condensation of $[Ta_6O_{19}]^{8-}$: Synthesis and Structure of $[\{(C_6H_6)Ru\}_2Ta_6O_{19}]^{4-}$ and $[\{(C_6H_6)RuTa_6O_{18}\}_2(\mu\text{-}O)]^{10-}$. *Inorg. Chem.* **2014**, *53*, 12791–12798.
49. Abramov, P.A.; Vicent, C.; Kompankov, N.B.; Gushchin, A.L.; Sokolov, M.N. Platinum polyoxoniobates. *Chem. Commun.* **2015**, *51*, 4021–4023.
50. Miras, H.N.; Wilson, E.F.; Cronin, L. Unravelling the complexities of inorganic and supramolecular self-assembly in solution with electrospray and cryospray mass spectrometry. *Chem. Commun.* **2009**, 1297–1311.
51. Sokolov, M.N.; Adonin, S.A.; Abramov, P.A.; Mainichev, D.A.; Zakharchuk, N.F.; Fedin, V.P. Self-assembly of polyoxotungstate with tetrarhodium-core: Synthesis, structure and ^{183}W NMR studies. *Chem. Commun.* **2012**, *48*, 6666–6668.
52. Ray, S.K. Synthesis of a Te dodecaniobate. *J. Ind. Chem. Soc.* **1976**, *53*, 1238–1239.
53. Son, J.-H.; Wang, J.; Osterloh, F.E.; Yu, P.; Casey, W.H. A tellurium-substituted Lindqvist-type polyoxoniobate showing high H_2 evolution catalyzed by tellurium nanowires via photodecomposition. *Chem. Commun.* **2014**, *50*, 836–838.

54. Nyman, M.; Bonhomme, F.; Alam, T.M.; Parise, J.B.; Vaughan, G.M.B. $[SiNb_{12}O_{40}]^{16-}$ and $[GeNb_{12}O_{40}]^{16-}$: Highly Charged Keggin Ions with Sticky Surfaces. *Angew. Chem., Int. Ed.*, **2004**, *43*, 2787–2792.
55. Anyushin, A.V.; Smolentsev, A.I.; Mainichev, D.A.; Vicent, C.; Gushchin, A.L.; Sokolov, M.N.; Fedin, V.P. Synthesis and characterization of a new Keggin anion: $[BeW_{12}O_{40}]^{6-}$. *Chem. Commun.* **2014**, *50*, 9083.
56. Black, J.R.; Nyman, M.; Casey, W.H. Kinetics of ^{17}O-exchange reactions in aqueous metal-oxo nanoclusters. *Geochim. Cosmochim. Acta* **2006**, *70*, A53-A53.
57. Nelson, W.H.; Tobias, R.S. Polyanions of the Transition Metals. II. Ultracentrifugation of Alkaline Tantalum(V) Solutions; Comparison with Light Scattering. *Inorg. Chem*. **1964**, *3*, 653–658.
58. Spinner, B.; Kheddar, N. Nouveaux isopolyanions du tantale V. *Comp. Rend*. **1969**, *268C*, 1108–1111.
59. Arana, G.; Etxebarria, N.; Fernandez, L.A.; Madariaga, J.M. Hydrolysis of Nb(V) and Ta(V) in aqueous KCl at 25 °C. Part II: Construction of a thermodynamic model for Ta(V). *J. Solution Chem*. **1995**, *24*, 611–622.
60. Matsumoto, M.; Ozawa, Y.; Yagasaki, A. Which is the most basic oxygen in $[Ta_6O_{19}]^{8-}$?—Synthesis and structural characterization of $[H_2Ta_6O_{19}]^{6-}$. *Inorg. Chem. Commun,* **2011**, *14*, 115–117.
61. Fullmer, L.B.; Molina, P.I.; Antonio, M.R.; Nyman, M. Contrasting ion-association behaviour of Ta and Nb polyoxometalates. *Dalton Trans.* **2014**, *43*, 15295–15299.
62. Deblonde, G.J.P.; Moncomble, A.; Cote, G.; Belair, S.; Chagnes, A. Experimental and computational exploration of the UV-visible properties of hexaniobate and hexatantalate ions. *RSC Adv.* **2015**, *5*, 7619–7627.
63. Maekawa, M.; Ozawa, Y.; Yagasaki, A. Icosaniobate: A New Member of the Isoniobate Family *Inorg. Chem.* **2006**, *45*, 9608–9609.
64. Matsumoto, M.; Ozawa, Y.; Yagasaki, A. Reversible dimerization of decaniobate. *Polyhedron* **2010**, *29*, 2196–2201.
65. Tsunashima, R.; Long, D.L.; Miras, H.N.; Gabb, D.; Pradeep, C.P.; Cronin, L. The Construction of High-Nuclearity Isopolyoxoniobates with Pentagonal Building Blocks: $[HNb_{27}O_{76}]^{16-}$ and $[H_{10}Nb_{31}O_{93}(CO_3)]^{23-}$. *Angew. Chem. Int. Ed.* **2010**, *49*, 113–116.
66. Villa, E.M.; Ohlin, C.A.; Rustad, J.R.; Casey, W.H. Isotope-Exchange Dynamics in Isostructural Decametalates with Profound Differences in Reactivity *J. Am. Chem. Soc.* **2009**, *131*, 16488–16492.
67. Villa, E.M.; Ohlin, C.A.; Casey, W.H. Oxygen-Isotope Exchange Rates for Three Isostructural Polyoxometalate Ions. *J. Am. Chem. Soc.* **2010**, *132*, 5264–5272.
68. Bannani, F.; Floquet, S.; Leclerc-Laronze, N.; Haouas, M.; Taulelle, F.; Marrot, J.; Kögerler, P.; Cadot, E. Cubic Box *versus* Spheroidal Capsule Built from Defect and Intact Pentagonal Units. *J. Am. Chem. Soc*. **2012**, *134*, 19342–19345.
69. Van Lokeren, L.; Cartuyvels, E.; Absillis, G.; Willema, R.; Parac-Vogt, T.N. Phosphoesterase activity of polyoxomolybdates: as a tool for obtaining insights into the reactivity of polyoxometalate clusters. *Chem. Commun.* **2008**, 2774–2776.

70. Lemonnier, J.-F.; Floquet, S.; Kachmar, A.; Rohmer, M.-M.; Bénard, M.; Marrot, J.; Terazzi, E.; Piguet, C.; Cadot, E. Host–guest adaptability within oxothiomolybdenum wheels: structures, studies in solution and DFT calculations. *Dalton Trans.* **2007**, 3043–3054.
71. Sakurai, N.; Kadohata, K.; Ichinose, N. Application of high-speed liquid chromatography using solvent extraction of the molybdoheteropoly yellow to the determination of microamounts of phosphorus in waste waters. *Fresenius' Z. Anal. Chem.* **1983**, *314*, 634–637.
72. Kirk, A.D.; Riske, W.; Lyon, D.K.; Rapko, B.; Finke, R.G. Rapid, high-resolution, reversed-phase HPLC separation of highly charged polyoxometalates using ion-interaction reagents and competing ions. *Inorg. Chem.* **1989**, *28*, 792–797.
73. Hettiarachichi, K.; Ha, Y.; Tran, T.; Cheung, A.P. Application of HPLC and CZE to the analysis of polyoxometalates. *J. Pharm. Biomed. An*. **1995**, *13*, 515–523.
74. Oliveri, A.F.; Elliott, E.W.; Carnes, M.E.; Hutchison, J.E.; Johnson, D.W. Elucidating Inorganic Nanoscale Species in Solution: Complementary and Corroborative Approaches. *ChemPhysChem* **2013**, *14*, 2655–2661.